PNAS
www.pnas.org

Supplementary Information for

Underactuated fluidic control of a continuous multistable membrane

Ofek Peretz,Anand Kumar Mishra,Robert F. Shepherd,Amir D. Gat

[1]To whom correspondence should be addressed. E-mail: ofekperetz@campus.technion.ac.il

This PDF file includes:

Other supplementary materials for this manuscript include the following:

Movies S1 to S2

Supporting Information Text

1. Asymptotic expansion

Scaling the governing equations [Eq. (3)-Eq. (5) in the paper] according to the lubrication approximation, and choosing to base scaling on state (1) (see Fig. 2), the corresponding normalized variables are

$$X = \frac{x}{l}, \quad T = \frac{t}{t^*}, \quad P = \frac{p}{p^*}, \quad Q = \frac{q}{w\bar{h}_1 u^*}. \tag{1}$$

Substituting dimensionless variables into the integral mass-conservation yields

$$a_1 \frac{p^*}{t^*}\frac{\partial P}{\partial T} + \frac{w\bar{h}_1 u^*}{l^*}\frac{\partial Q}{\partial X} = 0, \tag{2}$$

and substituting into equation Stokes equation yields,

$$u^*\bar{h}wQ = -\frac{p^* w\tilde{h}_1^3}{l12\mu}\frac{\partial P}{\partial X}. \tag{3}$$

Scaling analysis of Eq. (3) and Eq. (2) yields

$$u^* = \frac{p^*\bar{h}_1^2}{l12\mu}, \quad t^* = \frac{l^2 12\mu}{w\tilde{h}_1^3}a_1, \tag{4}$$

where p^* is defined by the characteristic snap-through pressures of the channel. The above equations focused on state (1) and were scaled accordingly. Keeping the above scaling, and performing substitution of Eq. (4) into Eq. (2) for both states (1) and (3), yields the linearized governing equations of both states via

$$\frac{\partial P_i}{\partial T} = \alpha_i \frac{\partial}{\partial X}\left(\frac{\partial P_i}{\partial X}\right) \tag{5a}$$

where

$$\alpha_1 = 1, \quad \alpha_3 = \frac{\tilde{h}_1^3 a_1}{\tilde{h}_3^3 a_3} \tag{5b}$$

with the initial and boundary conditions

$$P_1\left(0, T>0\right) = F(T), \quad P_3(X,0) = P_1\left(X,0\right) = 0,$$
$$P_1\left(X_s^-, T\right) = P_3\left(X_s^+, T\right) = P_s, \quad P_3\left(X\to\infty, T\right) = 0 \tag{6}$$

where P_s is the scaled snapping pressure (and may represent either P_s^{up} or p_s^{down}, see Fig. 1). In addition to the above conditions, applying integral mass conservation on the transition region located at X_s, and limiting the configuration to sufficiently small transition region (see Fig. 2) yields the mass-conservation condition at the transition region

$$q(x_s^-) - (a_1 p_s + w\bar{h}_1)\frac{\partial x_s}{\partial t} = q(x_s^+) - (a_3 p_s + w\bar{h}_3)\frac{\partial x_s}{\partial t}. \tag{7}$$

Substituting Eq. (3) and normalizing the equation according to Eq. (1), yields

$$\left.\frac{\partial P_1}{\partial X}\right|_{X=X_s^-} - \frac{\tilde{h}_3^3}{\tilde{h}_1^3}\left.\frac{\partial P_3}{\partial X}\right|_{X=X_s^+} = \frac{\partial X_s}{\partial T}\left(P_s\frac{a_3-a_1}{a_1} + \frac{w\bar{h}_3 - w\bar{h}_1}{p^* a_1}\right), \tag{8}$$

which provides an additional condition which allows obtaining the location of the transition region $X_s(T)$.

The set of equations Eq. (5) resembles the case of one-dimensional heat transfer involving a phase change, known as the Stefan problem. Each of the two regions is governed by a heat equation, with a discontinuity of the coefficients in each region and a moving boundary location between the regions. The heat equation governing both regions readily allows transformation to a self-similar form by the substitution,

$$\eta_i = \frac{X}{2\sqrt{\alpha_i T}} \tag{9}$$

yielding

$$2\eta_i\frac{dP_i}{d\eta} + \frac{d^2 P_i}{d\eta^2} = 0. \tag{10}$$

The above self-similar heat equation is integrable. Integration and determining the integration coefficients by applying boundary and initial conditions Eq. (6) yields the self-similar result of

$$P_1\left(X,T\right) = 1 + \frac{P_s - 1}{\mathrm{erf}\left(\beta\right)}\mathrm{erf}\left(\frac{X}{2\sqrt{\alpha_1 T}}\right), \tag{11a}$$

$$P_3(X,T) = \frac{1-\mathrm{erf}\left(\frac{X}{2\sqrt{\alpha_3 T}}\right)}{1-\mathrm{erf}\left(\beta\sqrt{\frac{\alpha_1}{\alpha_3}}\right)}P_s, \tag{11b}$$

$$X_s = 2\beta\sqrt{\alpha_1 T}, \tag{11c}$$

where β is a constant still to be determined. To calculate β, the expressions obtained to the pressure in both regions Eq. (11) are substituted into the Eq. (7) boundary condition, yielding the additional relation

$$\frac{P_s-1}{\mathrm{erf}(\beta)}\exp\left(-\beta^2\right) + \frac{\tilde{h}_3^3}{\bar{h}_1^3}\sqrt{\frac{\alpha_1}{\alpha_3}}P_s\frac{\exp\left(-\beta^2\frac{\alpha_1}{\alpha_3}\right)}{1-\mathrm{erf}\beta\sqrt{\frac{\alpha_1}{\alpha_3}}} + \beta\sqrt{\pi}\alpha_1 k = 0, \tag{12a}$$

where

$$k = -\left(P_s\frac{a_3-a_1}{a_1} + \frac{w\bar{h}_3 - w\bar{h}_1}{p^* a_1}\right). \tag{12b}$$

Solution of the self-similar profile define in Eq. (11a)-Eq. (11b) requires obtaining β from an implicit relation, defined by Eq. (12). While exact solution of Eq. (12) is not available, asymptotic approximation will be presented in the following sections. In order to present results from Eq. (11), the propagation rate parameter β was calculated numerically from equation Eq. (12) using a commercially available code (MATHEMATICA™) for various physical parameters. Self-similarity profiles are presented in Fig. S1, where characteristic values parameters were chosen as

$$P_s = 0.5, \quad k = 10, \quad \bar{h}_1/\bar{h}_3 = 2, \quad \tilde{h}_1/\tilde{h}_3 = 2, \quad \alpha_3/\alpha_1 = 8, \quad \alpha_1 = 1 \tag{13}$$

unless otherwise mentioned.

The implicit condition from which β is determined does not allow for an explicit solution, and thus direct insight regarding the effects of various physical parameters on the propagation of the transition region. We thus here use asymptotic expansions to derive an approximated, but hopefully a more insightful, expression for β. Numerical calculations of β from Eq. (12) are presented in Fig. S3(a-c). The computations show that $\beta \ll 1$ for $\kappa > 10$, which represent a large and useful physical region. We thus use the assumption of $\beta \ll 1$ as a basis for the approximation and the asymptotic expansions. We begin by developing Eq. (12) to a Taylor series around $\beta_0 = 0$, neglecting $O(\beta^2)$ terms,

$$(P_s-1)\left(\frac{\sqrt{\pi}}{2\beta} - \frac{\sqrt{\pi}\beta}{3}\right) + \sqrt{\frac{\alpha_1}{\alpha_3}}P_s\left(1+2\sqrt{\pi\frac{\alpha_1}{\alpha_3}}\beta\right)\frac{\tilde{h}_3^3}{\bar{h}_1^3} + \beta\sqrt{\pi\alpha_1}k = 0. \tag{14}$$

We multiply the above equation by β and substitute $\beta = \varepsilon B$, where $\varepsilon \ll 1$ and $B \sim O(1)$. Neglecting $O(\varepsilon^2)$ terms, we get

$$(P_s-1)\left(\frac{\sqrt{\pi}}{2} - \frac{\sqrt{\pi}\varepsilon^2 B^2}{3}\right) + \frac{\tilde{h}_3^3}{\bar{h}_1^3}\sqrt{\frac{\alpha_1}{\alpha_3}}P_s\left(\varepsilon B + 2\sqrt{\pi\frac{\alpha_1}{\alpha_3}}\varepsilon^2 B^2\right) + \varepsilon^2 B^2\sqrt{\pi}\alpha_1 k = 0. \tag{15}$$

Scaling arguments thus yields that $\beta \ll 1$ for $\kappa = K/\varepsilon^2$, where $K \sim O(1)$

$$(P_s-1)\left(\frac{\sqrt{\pi}}{2} - \frac{\sqrt{\pi}\varepsilon^2 B^2}{3}\right) + \frac{\tilde{h}_3^3}{\bar{h}_1^3}\sqrt{\frac{\alpha_1}{\alpha_3}}P_s\left(\varepsilon B + 2\sqrt{\pi\frac{\alpha_1}{\alpha_3}}\varepsilon^2 B^2\right) + B^2\sqrt{\pi}\alpha_1 K = 0. \tag{16}$$

We now introduce the regular asymptotic expansion $B = B_0 + \varepsilon B_1$. Following standard asymptotic approach, isolating the leading order equation and solving for B_0 gives

$$B_0 = \sqrt{\frac{1-P_s}{2\alpha_1 K}} \tag{17}$$

and similarly solution of the $O(\varepsilon)$ equation gives

$$B_1 = -\frac{\tilde{h}_3}{\tilde{h}_1}\sqrt{\frac{1}{\alpha_3\alpha_1\pi}}\frac{P_s}{2K}. \tag{18}$$

Thus, rearranging the equations, we get the approximated value of β in terms of the system physical parameters by

$$\beta_{asymptotic} = \sqrt{\frac{1-P_s}{2\alpha_1 k}} - \frac{\tilde{h}_3^3}{\tilde{h}_1^3}\sqrt{\frac{\alpha_1}{\alpha_3}}\frac{P_s}{2\sqrt{\pi}\alpha_1 k} \tag{19}$$

Figure S3(a-c) present the exact value of β calculated from Eq. (12) for various values of $\tilde{h}_1/\tilde{h}_3$, κ and P_s. The results indicate that β is sufficiently small at $\kappa > 10$ and $\tilde{h}_1/\tilde{h}_3 > 2$ in all the examined snapping pressures values of $P_s \in [0.25, 0.5, 0.75]$. In addition, panels (d-e) present comparison between the transition region location vs. time for both asymptotic expression obtained in equation Eq. (19) and the exact expression from numerical solution of Eq. (12) for parameters values defined in Eq. (13). Good agreement is obtained for all examined cases. As expected, larger values of κ provides smaller error. Panel (e) presents a quantitative comparison between asymptotic and exact expressions for β, for $\kappa \in [0.1 : 200]$, $\tilde{h}_1/\tilde{h}_3$ and $P_s = 0.5$. The logarithmic contour plot presents the errors defined by $|(\beta_{asymptotic} - \beta_{analytic})/\beta_{analytic}|$. The results show that the asymptotic expression is valid at $\kappa > 100$ and $\tilde{h}_1/\tilde{h}_3 > 1$, as expected.

2. Numeric β calculations

In order to assess the range of validity of the semi-infinite self-similar solution Eq. (11), equations [Eq. (5),Eq. (7)], along with the initial and boundary condition Eq. (6) were directly solved numerically for a finite length channel L = 0.8 m, with all other parameters as specified in equation Eq. (13). Figure S2 presents the numeric results obtained for the finite-length case. Figure S2(a) presents the pressure P vs. the streamwise direction X for different times. (b) presents the location of the transition region X_s vs. time. Analytic results are denoted by full lines and numeric computations are denoted by dashed lines. At early times, good agreement is obtained for the pressure profile. As time advances, and the transition region approaches the outlet, the error increases since the channel outlet affects the flow-field. Nonetheless, the self-similar solution gives good approximation for the location of the transition region X_s for all times.

$$err = \frac{1}{n}\sum_{i=1}^{n} Abs\left[\frac{X_s^n\left(i\cdot\Delta t\right) - X_s^a\left(i\cdot\Delta t\right)}{X_s^a\left(i\cdot\Delta t\right)}\right]\cdot 100\%, \quad \Delta t = \frac{1}{n}, \quad n = 100, \qquad [20]$$

where numeric results dented by X_s^n and asymptotic results denoted by X_a^n. The results show that for $\tilde{h}_1/\tilde{h}_3 > 2$ and $\kappa > 100$ the analytic results are accurate within an error of 10%.

3. Numerical calculations of p_s

The snapping pressure of a compressed elastic sheet is determined by the material properties and the geometry of the membrane. We here present two-dimensional numerical calculations of p_s for various values of membrane thickness and curve width. All other membrane properties and boundary conditions are held constant. The snapping pressure of a given geometry was calculated using Abaqus™FEM with an explicit solver. In the computations, a linear material model is assumed (elastic modulus of E = 100 MPa, density of ρ = 70 kg / m^3), in all simulations.

The initial geometry of the membrane was at the snapped-down state and it is then subjected to a uniform pressure acting on its internal surface (see Fig 1 right panel). Both sides of the membrane were clamped with a distance of 15.8 mm (identical to the channel width in the experiment). In each simulation the pressure was increased linearly until a snap-up occurred, the value of the pressure in this increment was measured as p_s. The same analysis was preformed for thickness values in the range of (0.1 - 2 mm) and membrane width divided by the gap between the vertical walls (Δw) in the range of (1.2-2.2).

Figure S4 presents the snapping pressure vs membrane thickness for different membrane widths. The analysis shows that, as expected, a higher curve ratio (membrane width divided by the gap between the vertical walls) results in higher snapping pressure. Similar behavior is observed for membrane thickness, in which higher thickness results in higher snapping pressures. The analysis shows that the effect of thickness variation has a greater impact than the membrane width.

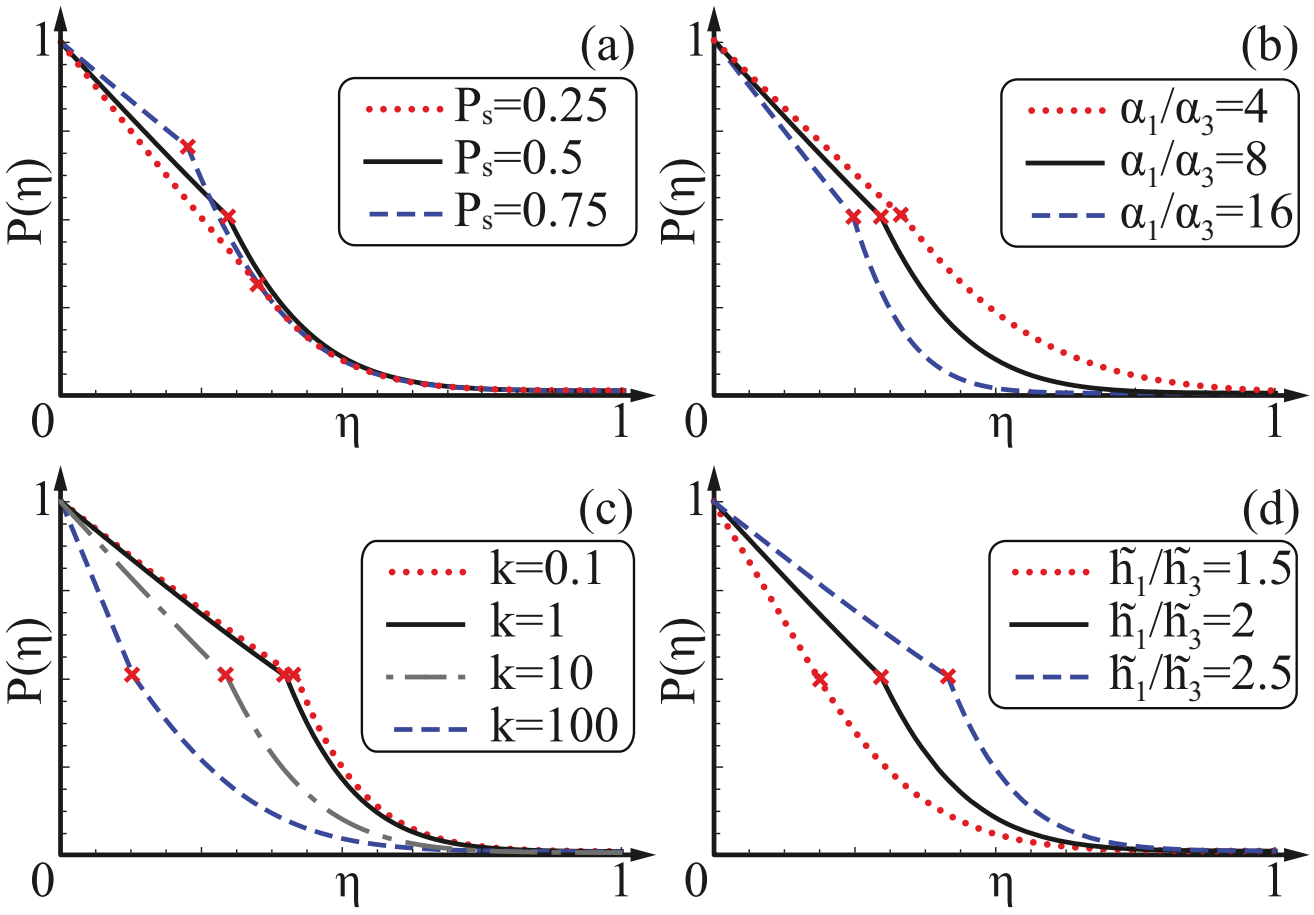

Fig. S1. Self-similar solutions for semi-infinite channels for various parameters values. In each panel, all parameters were kept constant according to Eq. (13) except for the variation of a single parameter: (a)- $P_s \in [0.25, 0.5, 0.75]$, (b) $\alpha_1/\alpha_3 \in [4, 8, 16]$, (c) $\kappa \in [0.1, 1, 10, 100]$, (d) $\tilde{h}_1/\tilde{h}_3 \in [1.5, 2, 2.5]$. In all cases, β was calculated numerically from equation Eq. (12).

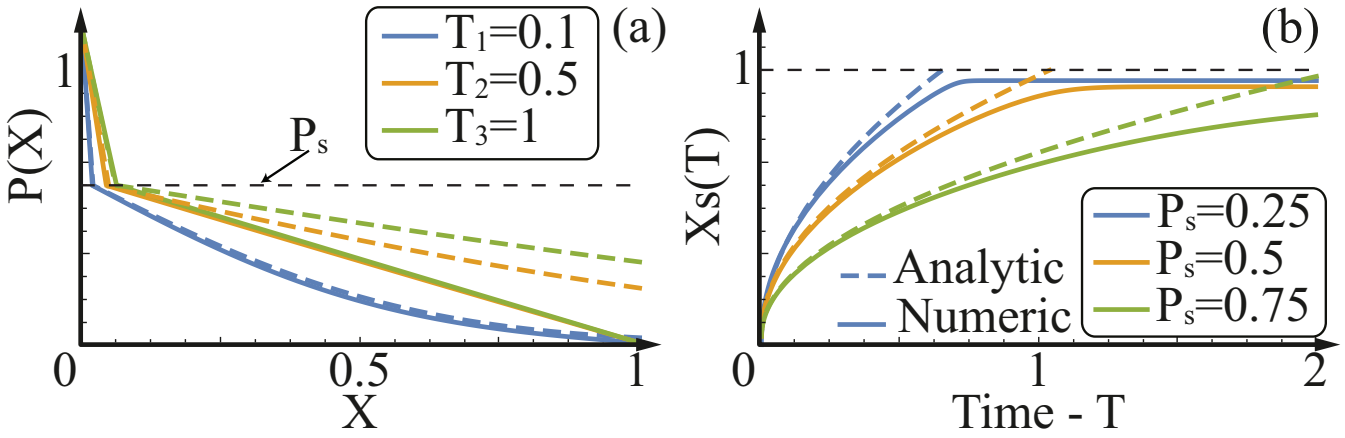

Fig. S2. Numeric solutions for finite-length channels, with comparison to the semi-infinite model. Panel (a) presents the pressure vs. the streamwise coordinate X for different times, for both analytic (full lines) and numeric (dashed lines) computations. Panel (b) compares the location of the transition region obtained by the numeric calculation along with the results from semi-infinite solution.

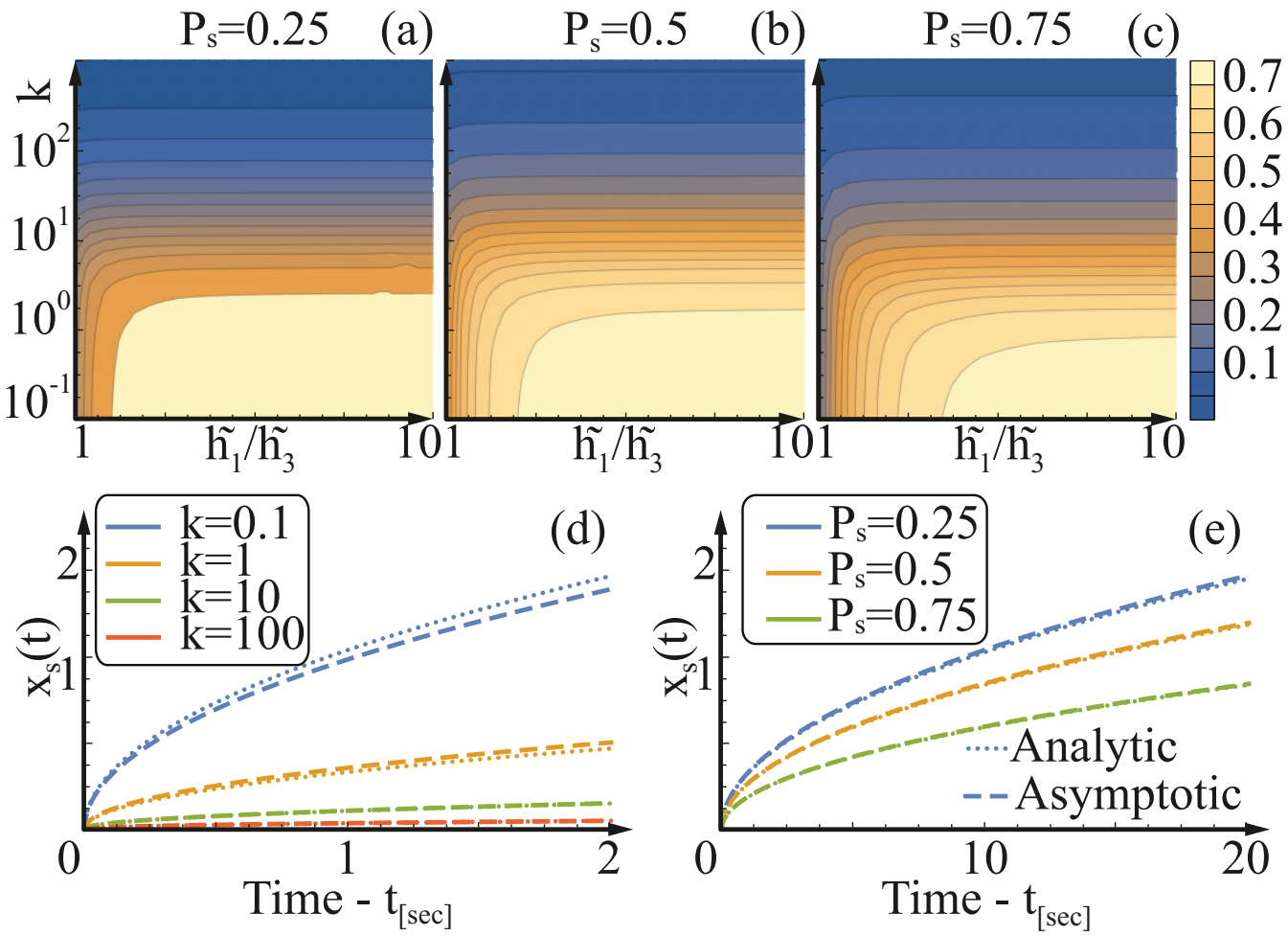

Fig. S3. Comparison between asymptotic and exact expressions for β for various cases. Panels (a-c) presents contour plot for β obtained from numerical solution of equation Eq. (12) for values range in $\kappa \in [0.1:200]$, $\tilde{h}_1/\tilde{h}_3 \in [1:10]$ and $P_s \in [0.25, 0.5, 0.75]$. Panels (d) and (e) presents transition region location $x_s(T)$ vs. time for asymptotic (dashed lines) and exact (dotted lines) expressions of β for $\kappa \in [0.1, 1, 10, 100]$ and $P_s \in [0.25, 0.5, 0.75]$. Panel (e) presents the value of $|\left(\beta_{asymptotic} - \beta_{analytic}\right)/\beta_{analytic}|$, a quantitative comparison between asymptotic and analytic expressions for β, for $\kappa \in [0.1:200]$, $\tilde{h}_1/\tilde{h}_3 \in [1:10]$ and $P_s = 0.5$.

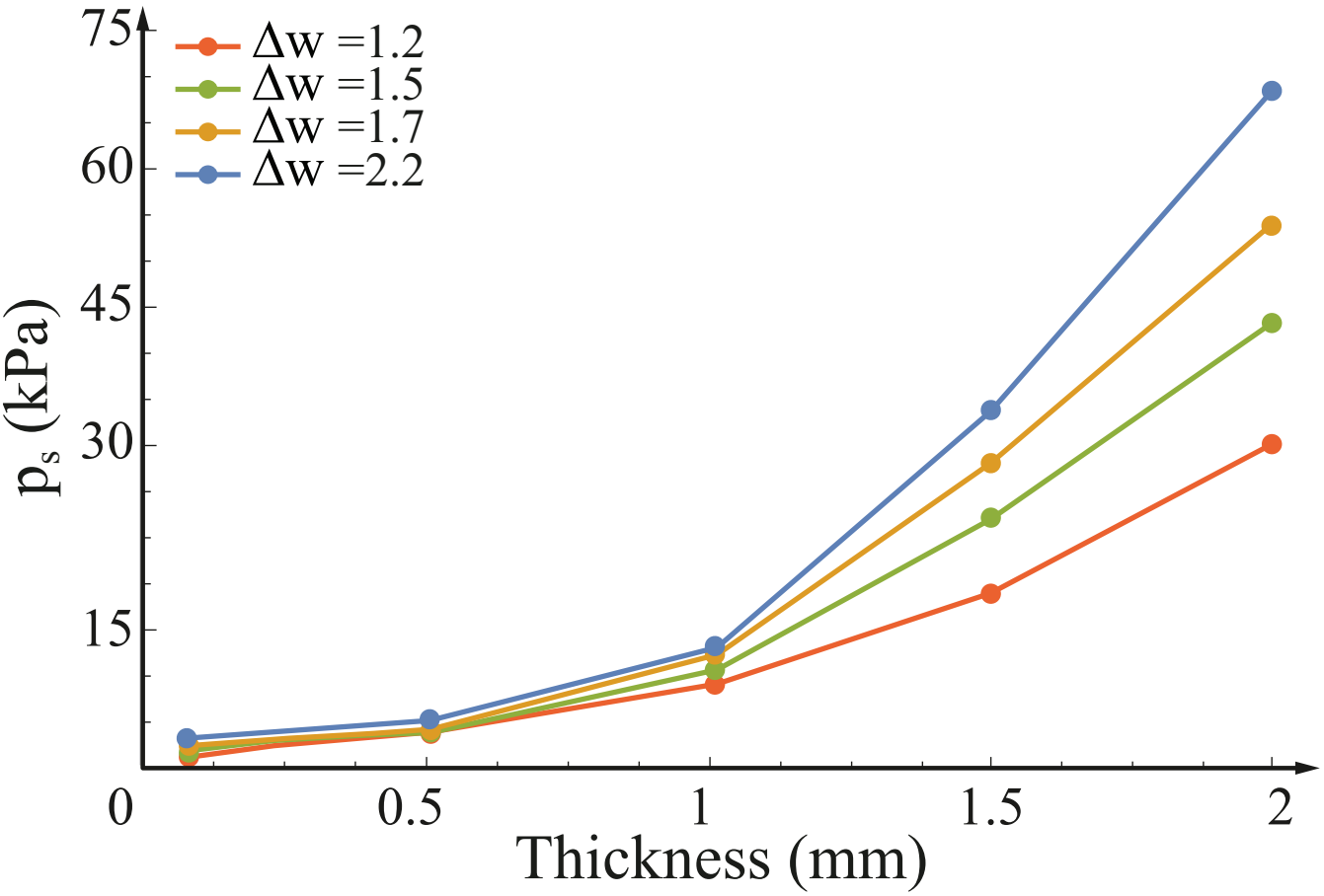

Fig. S4. Numeric parameter analysis of the snapping pressure vs membrane thickness. Numerical, Abaqus™FEM computations, results for the snapping pressure are presented for various values of membrane thickness and width. Each line presents results for different membrane width divided by the gap between the vertical walls (Δw

.

Movie S1. Patterning using various inlet pressure profiles - uniform membrane

Movie S2. Direct fluidic-induced patterning using various inlet pressure profiles - nonuniform membrane.

References